Foldable All-Textile Cavity-Backed Slot Antennas for Personal UWB Localization

Dries Van Baelen[1], Quinten Van den Brande[1], Sam Lemey[1], Jo Verhaevert[1]and Hendrik Rogier[1]

[1]IDLab, Department of Information Technology at Ghent University - imec

Key Points:

- Design and automated fabrication of a lightweight and mechanically flexible all-textile antenna for ultra-wideband
- Stable radiation pattern and impedance matching in proximity of human body and under mechanical bending
- High system fidelity factor (>94%) and localization accuracy in the order of 5 cm in relevant directions

Corresponding author: Dries Van Baelen, Dries.VanBaelen@UGent.be

Abstract

An all-textile multi-moded cavity-backed slot antenna has been designed and fabricated for body-worn impulse radio ultra-wideband (IR-UWB) operation in the [3744-4742.4] MHz frequency band, thereby covering Channels 2 and 3 of the IEEE 802.15.4a standard. Its light weight, mechanical flexibility and small footprint of 35 mm × 56 mm facilitate integration into textile for radio communication equipment for first aid responders, personal locator beacons and equipment for localization and medical monitoring of children or the elderly. The antenna features a stable radiation pattern and reflection coefficient in diverse operating conditions such as in free space, when subject to diverse bending radii, and when deployed on the torso or upper right arm of a test person. The high isolation towards the wearer's body originates from the antenna's hemispherical radiation pattern with a -3 dB beamwidth of 120° and a front-to-back-ratio (FTBR) higher than 11 dB over the entire band. Moreover, the antenna exhibits a measured maximum gain higher than 6.3 dBi and a radiation efficiency over 75%. In addition, orientation-specific pulse distortion introduced by the antenna element is analyzed by means of the System Fidelity Factor (SFF). The SFF of the communication link between two instances of this antenna is higher than 94% for all directions within the antenna's -3 dB beamwidth. This easily wearable and deployable antenna is suitable to support IR-UWB localization with an accuracy in the order of 5 cm.

1 Introduction

The promising ascent of the Internet of Things (IoT) includes an increasing demand for reliable and integrable Wireless Body Area Network (WBAN) systems (Chatterjee et al., 2017). To achieve a market breakthrough, these systems should be wearable in an unobtrusive and comfortable way (Agneessens et al., 2015; Lemey et al., 2018). Given their mechanical flexibility and the possibilities for unobtrusive on-body integration, textile implementations are promising candidates to fill in a WBAN system's antenna role (Skrivervik & Marrocco, 2015). In the last decade, a significant amount of research has been invested in the development of textile antennas, enabling applications for first aid responders (Castel et al., 2015; Dierck et al., 2013; Lilja et al., 2012), healthcare (Agneessens et al., 2013; Bait-Suwailam et al., 2019; Bharadwaj et al., 2017; Rogier et al., 2014), sports (Mandal et al., 2013), space (Kennedy et al., 2009), military (Kaija et al., 2010; Lee et al., 2016), RFID (Khan et al., 2019) and by extension the Internet of Things (IoT) (Lee & Choi, 2017; Lemey & Rogier, 2014; Loss et al., 2016). The opening of the 3.1-10.6 GHz UWB band along with the publication of the IEEE802.15.4 standard ("IEEE Standard for Local and metropolitan area networks–Part 15.4: Low-Rate Wireless Personal Area Networks (LR-WPANs)", 2011) creates possibilities which recently are being picked up by textile electronics developers.

UWB allows for very high data rates for close-range communication with excellent resilience against multipath effects (Adamiuk et al., 2012; Luo & Look Law, 2015), while using power levels close to the noise floor, thereby avoiding interference with narrowband systems (Kshetrimayum, 2009). This low power use is particularly favorable for body-worn systems considering their often limited availability of power (Agneessens et al., 2015). Furthermore, the high available bandwidth enables impulse radio ultra-wideband (IR-UWB) systems to use very narrow time-domain pulses, which allows for ranging at centimeter-scale accuracy (Alarifi et al., 2016; Ridolfi et al., 2018) with a high immunity against multipath fading (Kshetrimayum, 2009). Examples of applications include cyclist positioning systems using the Decawave's DW1000 IC (Minne et al., 2019), systems for respiration and heartbeat monitoring (Shen et al., 2018), drone localization (Lazzari et al., 2017) and breathing detection of victims buried under building rubble (Lv et al., 2014). To allow localization algorithms to provide accurate results, special care must be taken by the designer to mitigate the pulse distortion introduced by the antenna (Zwirello et al., 2012).

In the most recent years, numerous UWB textile antennas have been developed, of which many target the IEEE 802.15.4 frequency bands (Klemm & Troester, 2006; Samal et al., 2014; Yan et al., 2016; Yimdjo Poffelie et al., 2016; Zhong et al., 2017; Zhu & Langley, 2009). However, these antennas do not meet all applicable criteria for antenna deployment in a body-worn scenario for IR-UWB operation. From the time domain perspective, the pulse distortion introduced by the antenna should be reduced to the bare minimum (Zwirello et al., 2012). As of today, this issue is still underexposed in IR-UWB design for wearables. From the perspective of wearability, the antenna must exhibit a small footprint and should be mechanically flexible (Osman et al., 2012; Sanz-Izquierdo et al., 2007). In addition, effects such as bending and the presence of the human body should not adversely affect antenna performance (Hong et al., 2016; Liu et al., 2016). Furthermore, the aforementioned limited availability of power in body-worn systems requires a high radiation efficiency (Van Baelen et al., 2018). Moreover, the antenna's radiation pattern should remain stable over the targeted frequency band to mitigate orientation-specific pulse distortion (Rabah et al., 2015). Finally, in textile antenna design, the moisture regain of the materials applied as substrates should be limited to 3%, to avoid significant deviations in the substrate's dielectric permittivity (Hertleer et al., 2010). The design of a textile antenna system for reliable and high-accuracy IR-UWB applications should take all aforementioned specifications in account.

In this paper, the bandwidth enhancement technique proposed by Van den Brande et al. (2018) is combined with time and frequency co-simulation to design a wearable all-textile cavity-backed slot antenna for use in on-body IR-UWB systems. The antenna is developed on a substrate with a low moisture regain and manufactured using an accurate and reliable fabrication methodology for textile-based cavity-backed slot antennas (Van Baelen et al., 2019), to ensure stable behavior of the antenna materials and a reliable, accurate and automated fabrication process. This results in a small and flexible antenna in which only the connector is rigid. Measurements on a fabricated prototype show that the antenna's reflection coefficient with respect to 50 Ω remains below -10 dB over the 3744 MHz - 4742.4 MHz band when deployed in free space, when deployed on diverse locations on the human body and when subjected to diverse bending radii. Moreover, the antenna's radiation pattern is directed away from the wearer's body and remains stable over the entire frequency band for all investigated scenario's. Finally, for all relevant directions, the antenna's orientation specific pulse distortion is low, demonstrated by a System Fidelity Factor (SFF) higher than 94% as discussed in Section 4.2.

This paper is structured as follows. In Section 2, the design specifications are put forward, together with a discussion of the chosen antenna topology and its operation principle. Section 3 elaborates on the dedicated fabrication method for the production of all-textile cavity-backed Substrate Integrated Waveguide (SIW) antennas, and more specifically how it is applied to implement this design. Simulations have been performed in both time and frequency domain to meet the design goals. Time domain results and the final antenna dimensions are shown in Section 4. In Section 5, the results of the measurements, both in free space and on a human body, are discussed.

2 Antenna Design

This section discusses the antenna's design specifications in both frequency and time domain, along with the antenna topology chosen to meet these goals. Furthermore, the utilized antenna materials are briefly discussed.

2.1 Design specifications

The antenna is designed to cover both Channels 2 (3744 MHz - 4243.2 MHz) and 3 (4243.2 MHz - 4742.4 MHz) of the IEEE 802.15.4 standard for personal IR-UWB-based localization applications with an accuracy of at least 5 cm. Therefore, over both frequency

ranges, the magnitude of the reflection coefficient of the antenna with respect to 50 Ω should stay below -10 dB. Moreover, the radiation pattern and the gain should remain stable in these channels. Over the targeted frequency band, the broadside gain should vary no more than by 3 dB and the radiation efficiency should be at least 70%. These characteristics should be maintained when the antenna is deployed on the human body or when it is subjected to mechanical bending, which often occurs during deployment on the human body. In addition, a front-to-back-ratio (FTBR) higher than 6 dB is recommended to minimize absorption of antenna radiation by the human body. Increasing the FTBR not only decreases the wearer's radiofrequency-field exposure, but also improves the antenna's radiation efficiency. This is especially desirable because of the limited available power in body-worn applications. Minimizing coupling between the antenna and the wearer's body also results in a more stable radiation pattern and offers more options in terms of suitable antenna deployment on the body.

Furthermore, IR-UWB applications require minimal pulse distortion introduced by the transmit and receive antenna. Otherwise, the deformation of the received pulse may affect the localization algorithms, resulting in an inaccurate location estimation. Given that the propagation channel acts as a dispersive medium, pulse distortion should be considered at the system level, taking into account both transmit and receive antennas, as well as the wireless channel (Van den Brande et al., 2018). A useful figure of merit to express pulse distortion in the total localization system is the System Fidelity Factor (Quintero et al., 2011). For localization purposes, the SFF of the IR-UWB system is generally required to be larger than or equal to 90% for all relevant orientations of the receive antenna, with respect to the transmit antenna.

2.2 Antenna topology and materials

A cavity-backed slot antenna is adopted to satisfy all imposed design requirements and to facilitate an all-textile implementation. To implement such an antenna, a slot is cut out in a coaxially fed metallic cavity that is filled by a dielectric material. The metal cavity walls ensure that the slot is the only radiating part of the antenna, thereby directing the antenna radiation away from the human body. As radiating cavities typically exhibit a narrowband behaviour, the bandwidth enhancement technique proposed by Van den Brande et al. (2018), is applied to ensure that the antenna covers the entire frequency band, as elaborated in Section 2.3.

The complete implementation of the antenna in textile materials offers the mechanical flexibility necessary in body-worn systems and allows for integration into the garments of the user. As a conductive material, copper-plated Pure Copper Taffeta electrotextile by Less EMF (`lessemf.com`) is used. This material has excellent handling characteristics facilitating antenna fabrication, and offers a very low sheet resistivity of 0.05 Ohm/sq, which reduces the conductivity losses of the antenna and thus favorably impacts the radiation efficiency. The dielectric substrate is implemented in a closed-cell expanded rubber material by Javaux (`javaux.com`). With a thickness of 4 mm and excellent recovery from mechanical compression it offers a sufficiently large and stable thickness required for reliable broadband cavity antenna design. Furthermore, its low moisture regain makes its electromagnetic characteristics very resistant against humidity variations. This material is commonly applied as a protective foam in firefighter jackets owing to its resistance against water, heat, fire and a diverse spectrum of chemical compounds.

2.3 Operation principle

Since radiating cavities are typically very narrowband, we apply the bandwidth enhancement technique proposed by Van den Brande et al. (2018). In this approach, the open sides of two half-mode cavities with comparable resonance frequencies are brought

in close proximity, as shown in Figure 1a. Thereby, both half mode cavity resonators are coupled, resulting in mode bifurcation, which distinctly moves both resonances apart (Hong & Lancaster, 1996). By thorough computer-aided optimization of the half-mode cavity dimensions, along with an adjustment of the separation between both and, thus, the coupling between them, a precise control of the location of both resonance frequencies can be obtained. This allows for a complete coverage of the frequency band of operation. The cavity is excited by a coaxial feed, judiciously placed into one of the half mode cavities (Figure 1b). By connecting the cavity's top and bottom plane to the feed's central and outer conductors respectively, a loop is formed, creating a magnetic field in the cavity that couples to the resonant modes of both half-mode subcavities (Van Baelen et al., 2018). Therefore, the antenna's E-field lies in the XZ-plane, as shown in Figure 1c, and the H-field lies in the YZ-plane. As such, the antenna is linearly polarized.

In a realistic deployment scenario, the electrotextile forming the SIW cavity tends to crumple when it is subject to bending, causing delamination of the electrotextile and the substrate. To avoid this, apertures have been introduced in the vertical cavity walls to ensure that the bending of the vertical cavity walls occurs only along these apertures, thereby reducing stress on the electrotextile. This is illustrated in Figure 1c. To minimize radiation losses, the recommended ratio S/D between the width of the apertures and the width of the electrotextile slabs should be equal to or lower than 1 (Bozzi et al., 2011).

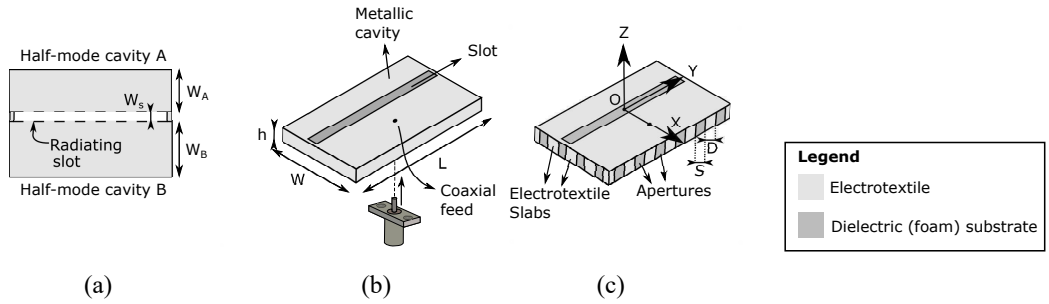

Figure 1. Coupled half-mode cavity design.

To accommodate the need for fabrication convenience and automation, together with demanding requirements for wearability and, hence, textilization of the design, the dedicated fabrication process proposed by Van Baelen et al. (2018), is applied, as further elaborated in Section 3.

3 Fabrication method

The accurate fabrication process can be summarized in four main steps. First, the electrotextile is vacuum laminated to a thermally activated sheet adhesive. Next, both the substrate and the electrotextile are laser cut into their respective shapes. A laser cutter offers the computerized sub-millimeter accuracy unachievable by hand. Furthermore, cutting with scissors or scalpels involves a significant risk of leaving loose strands of the electrotextile fabric. This is especially harmful when these strands would be left in critical areas such as the radiating slot or the connector aperture, not to mention the possibility of short circuits caused by the filaments. Note that, as the electrotextile is cut in one single piece, it can simply be folded around the substrate in a later step, thereby significantly reducing potential misalignments of the top and bottom planes. The 4 mm thick substrate is laser cut in a rectangular patch of 56 mm $\times$ 35 mm. The shape of the electrotextile cut is displayed in Figure 2. Next, the glue carrier sheet is removed, leaving the glue behind on the laser-cut electrotextile patch. After careful alignation, the sub-

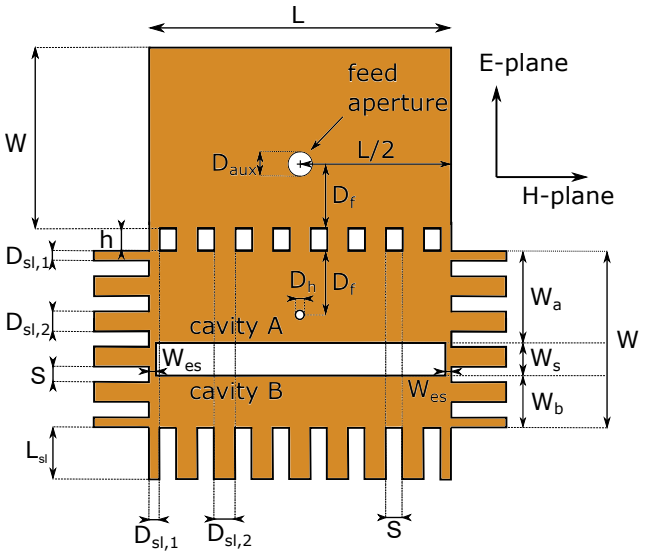

Figure 2. Electrotextile dimensions: L = 56 mm, W = 35 mm, W_a = 10.5 mm, W_b = 20 mm, W_s = 4.5 mm, h = 4 mm, D_f = 15 mm, D_{aux} = 5 mm, D_h = 1.27 mm, $D_{sl,1}$ = 2 mm, $D_{sl,2}$ = 4 mm, S = 3 mm, L_{sl} = 10 mm, W_{es}= 1 mm.

Figure 3. Final antenna design. Left: Slot plane. Right: Back plane.

strate and the electrotextile patch slot plane are glued together by a textile heat transfer press, which activates the glue. Then, the rest of electrotextile can be wrapped around the substrate, which forms the final cavity as shown in Figure 1c. Note that in this way, the vertical walls of the cavity contain evenly spaced apertures, thereby creating a rectangular SIW cavity. In a final step, the assembly of the antenna is concluded by placing the connector. Suitable apertures in the electrotextile were implemented during the laser cutting process, allowing to punch an appropriately trimmed SMA connector through the substrate. Now, the ground pads of the connector are soldered to the antenna back plane and the center conductor is soldered to the slot plane. This results in the final prototype shown in Figure 3.

4 Simulation and Optimization

To fulfill the design requirements specified in Section 2, both frequency-domain optimizations and time-domain simulations have been carried out. In Section 4.1, the influence of the antenna parameters on impedance matching and the location of the resonance frequencies is discussed. Section 4.2 elaborates on the time domain pulse distortion caused by the antenna and discusses the simulated distance estimation errors.

4.1 Frequency domain simulations

The antenna has been simulated and optimized by using CST Microwave Studio. By performing a thorough parametric analysis, the design goals as stated in Section 2.1 are met, as will be shown in Section 5. The width of both subcavities (ie. W_a and W_b as seen in Figure 2) are the primary parameters to fix the antenna resonance frequencies, along with the length of the cavity L. The latter and the placement of the feed D_f are used to match the antenna to the required impedance level over the entire operating band. To achieve the required bandwidth, the amount of coupling between both half-mode cavities is optimized via the slot parameters W_s and W_{es}. Although lower values of W_{es} cause a larger impedance matching bandwidth, a trade-off must be made to ensure the mechanical integrity of the antenna, since setting W_{es} to zero would remove a necessary support structure keeping some vertical electrotextile walls in place. Therefore, a sufficiently large value for W_{es} should be selected. For this, $W_{es} = 1$ mm is chosen.

All the aforementioned parameters have been optimized to comply with impedance matching goals, while maintaining a stable desired radiation pattern over the target frequency band and meeting the time domain requirements described in Section 4.2. Well-considered dimensions for $D_{sl,1}$, $D_{sl,2}$ and S ensure that radiation losses through the vertical cavity walls are negligible while guaranteeing mechanical flexibility. The resulting simulated reflection coefficient and radiation pattern of the proposed antenna are shown in Section 5 together with the measurement results.

4.2 Time domain simulations

Next, the orientation-specific pulse distortion of our all-textile antenna element is analyzed by means of the SFF, defined by Quintero et al. (2011) as:

$$SFF = \max_t \left| \frac{\int_{t_0}^{t_n} T_s(\tau) R_s(\tau + t) d\tau}{\sqrt{\int_{t_0}^{t_n} T_s^2(\tau) d\tau \int_{t_0}^{t_n} R_s^2(\tau) d\tau}} \right|,$$

where T_s(t) and R_s(t) represent the pulse at the transmit antenna's port and the receive antenna's port, respectively. As such, the antenna is analyzed in a complete transmit-receive antenna system. In this paper, our all-textile UWB antenna element is used both as a transmit and receive antenna. Then, the procedure outlined in Quintero et al. (2011) is exploited to calculate the antenna system's SFF when the receive antenna is rotated in its E- and H-plane, respectively, while the transmit antenna is transmitting along broadside. As an input pulse, the default output pulse of the Decawave DW1000 chipset when operating in Channel 2 is used. The resulting SFF in the relevant hemisphere is displayed in Figure 4, which is indeed larger than 90% for all relevant orientations of the receive antenna. As such, the pulse distortion due to the antenna characteristics is small enough to enable localization algorithms to provide accurate location estimations. In a subsequent step, the distance estimation error is determined to be in the order of magnitude of 5 cm as can be seen in Figure 5.

5 Measurements

This section discusses the measured figures of merit of a fabricated prototype both in free space and in two human body deployment scenarios. Furthermore, the impact of mechanical bending on antenna performance has been investigated.

Both the reflection coefficient and the radiation pattern measurements were performed using an Agilent N5242A PNA-X Microwave Network Analyzer (Agilent Technologies, `https://www.agilent.com/`). For the radiation pattern measurements the an-

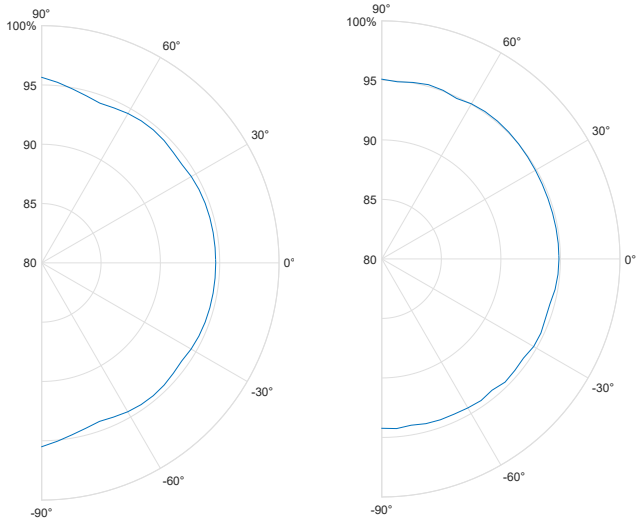

Figure 4. SFF using the pulse measured on a DW1000 IC operating in Channel 2. Left: SFF [%] in H-plane. Right: SFF [%] in E-plane.

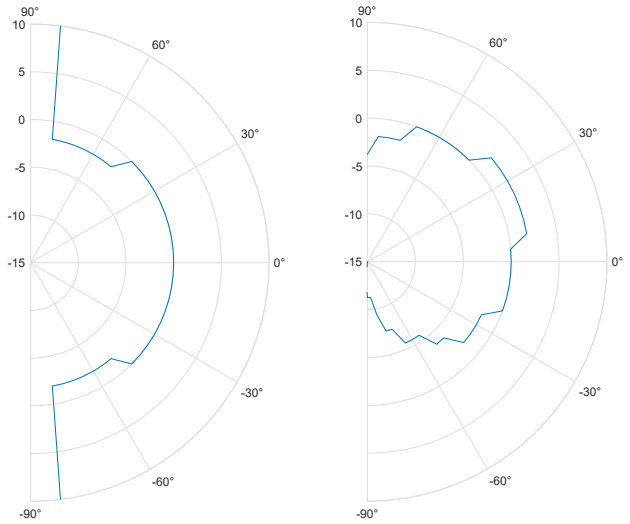

Figure 5. Distance estimation error. Left: DEE [cm] in H-plane. Right: DEE [cm] in E-plane.

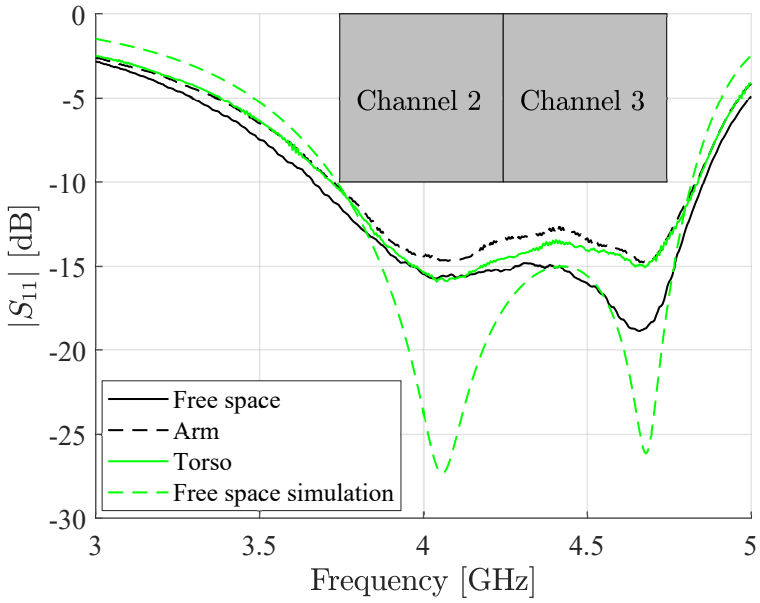

Figure 6. Magnitude of the measured reflection coefficient $|S_{1,1}|$ of the antenna in different deployment scenarios, in comparison to the simulated free space reflection coefficient.

tenna has been mounted on a Orbit/FR DBDR antenna positioning system (`http://www.orbitfr.com/`) in a full anechoic chamber.

In Figure 6, the simulated reflection coefficient is compared to the measured reflection coefficients in a stand-alone free space environment and in an on-body deployment scenario. Here, the antenna has been outfitted on a test person, having a size of 1.90 m and a mass of 85 kg. Measurements were performed when the antenna was placed on the torso and the upper right arm of the test person, respectively.

Both in simulations and measurements, the two resonances are clearly visible, providing an impedance bandwidth spanning the entire targeted frequency band. The measured free space fractional bandwidth of 27.9% qualifies this antenna as an UWB antenna. Furthermore, there is good correspondence between the resonance frequencies of the free space measurement and the resonance frequencies of the on-body measurements. Differences between simulation and measurements originate from fabrication tolerances and deployment conditions that slightly differ from the exact free space conditions assumed by the simulator. Furthermore, the electromagnetical properties of the applied materials vary slightly from batch to batch. Comparison between the measured scenarios proves that the influence of the human body on the antenna's reflection coefficient is indeed very limited.

Figure 7 shows the measured free space radiation patterns in the E-plane and H-plane, respectively. Table 1 summarizes the most important figures of merit related to the radiation pattern. Both the antenna's maximum gain and FTBR remain stable over the entire frequency band. Moreover, the measured radiation efficiency is higher than 75%. Owing to a large FTBR and a 3 dB-beamwidth of 120° centered around broadside, the radiation pattern experiences little influence from the proximity of the human body, as seen in Figure 8. Here, the radiation patterns at 4243.2 MHz, resulting from simulation in free space stand-alone conditions, measurement in free space conditions and when deployed on body show good agreement. Figure 9 shows the radiation patterns of

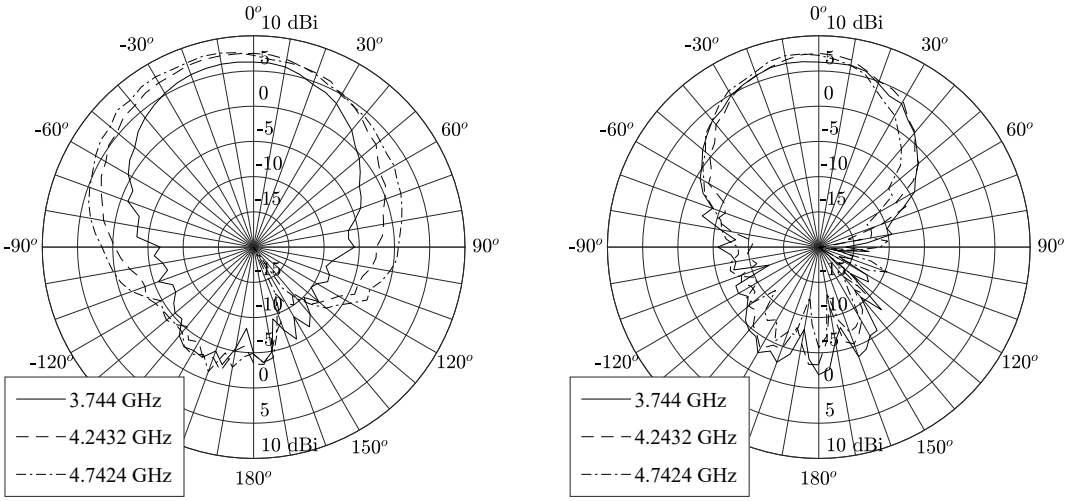

Figure 7. Free space radiation pattern. Left: E-plane, Right: H-plane.

the antenna while deployed on the torso and the arm of the test person, respectively. Because the positioning accuracy of a test person is prone to small errors, the maxima of the main lobes have slightly shifted.

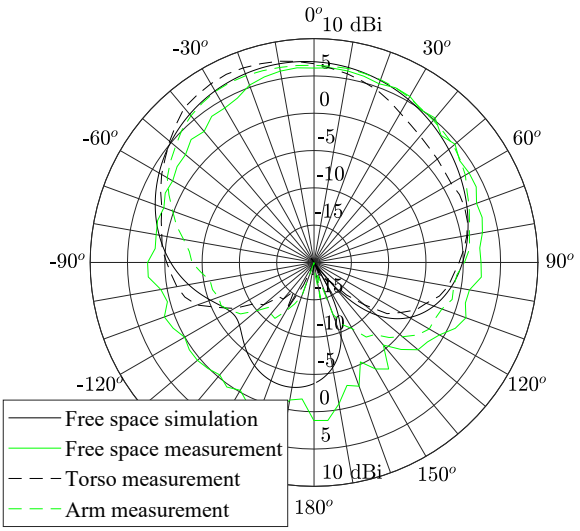

Figure 8. E-plane radiation pattern in different deployment scenarios, at 4243.2 MHz

Additional free space measurements have been performed while the antenna was subjected to mechanical bending around the X-axis shown in Figure 1c, which lies in the antenna's E-plane. For this, bending ratios frequently encountered on the human body

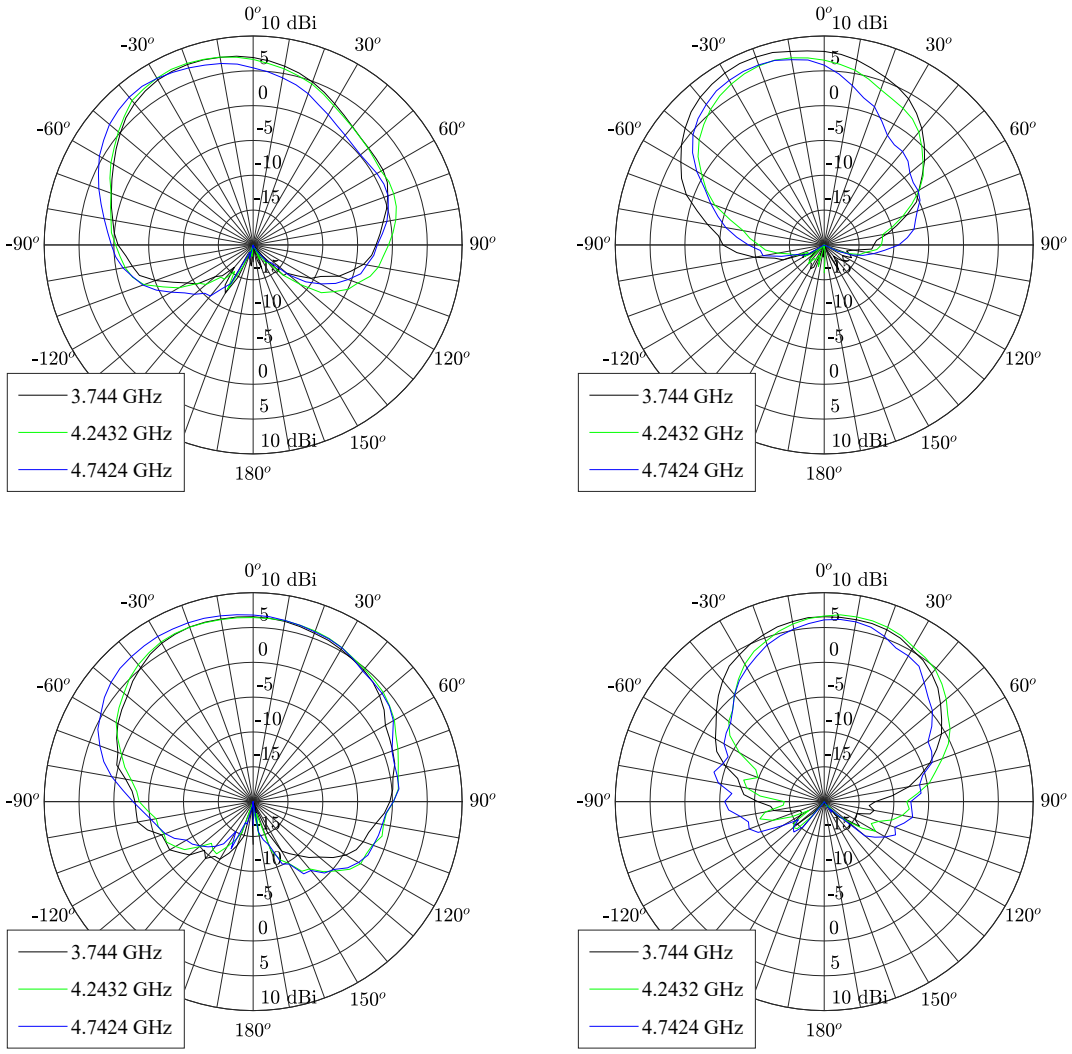

Figure 9. Radiation pattern on body. Top left: Torso E-plane, top right: Torso H-plane. Bottom left: upper right arm E-plane, bottom right: upper right arm H-plane.

have been chosen. Figure 10 compares the reflection coefficients of diverse bending radii. The influence of bending on the radiation pattern can be seen in Figure 11. These figures show that the antenna characteristics remain stable under bending. Only under the small bending radius of 4 cm, the resonance frequencies shift such that the complete UWB frequency band is no longer fully covered.

6 Conclusions

An all-textile multi-moded cavity-backed slot antenna that covers channels 2 and 3 of the IEEE 802.15.4 standard has been proposed for on-body deployment in personal IR-UWB-based localization applications. The magnitude of the reflection coefficient with respect to 50 Ω remains lower than -10 dB over a fractional bandwidth of 27.9%, thereby qualifying the antenna as an UWB antenna. The measured FTBR of 11 dB indicates that the antenna's radiation pattern is directed away from the wearer's body. Therefore,

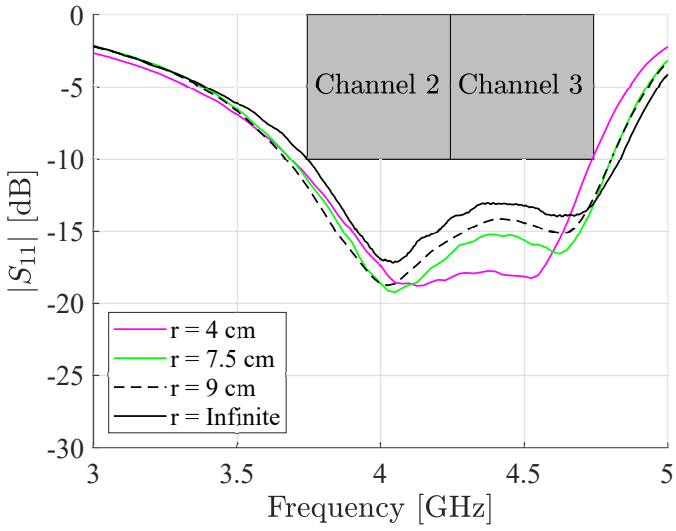

Figure 10. Magnitude of the measured reflection coefficient $|S_{1,1}|$ of the antenna while subject to mechanical bending, for different bending radii r, along the E-plane axis.

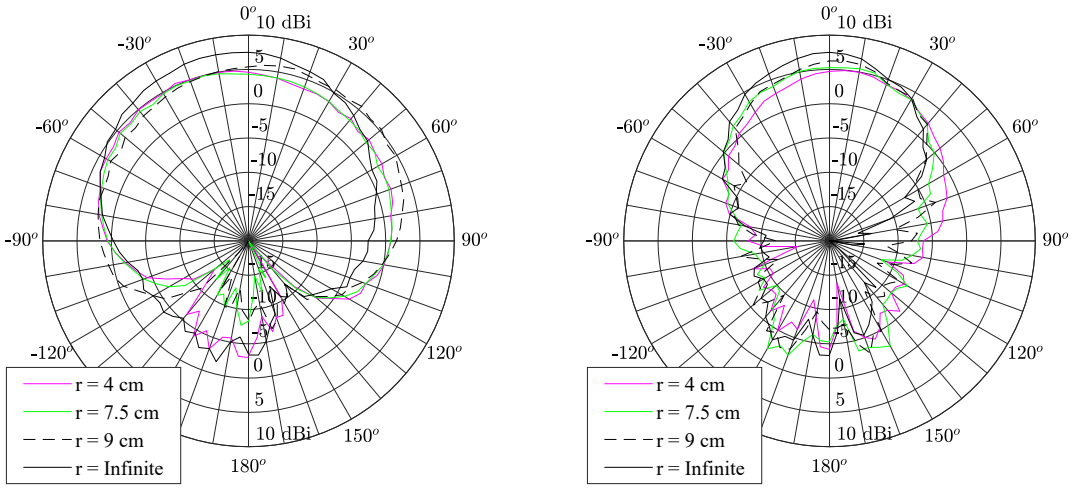

Figure 11. Measured radiation pattern under diverse bending radii, at 4243.2 MHz. Left: E-plane, Right: H-plane

less power is dissipated in the wearer's body in comparison with more omnidirectional antennas, resulting in a more efficient use of available power and reducing the wearer's radio field exposure. The antenna's reflection coefficient and radiation pattern have been investigated in free space, when the antenna was deployed on the torso and upper right arm of a test person, respectively, and in free space when bent over diverse bending radii. Measurements show that both the reflection coefficient and the radiation pattern experience limited influence from bending or proximity of the human body, illustrating the low coupling between the antenna and the human body. Simulations in the time-domain show the antenna's suitability for IR-UWB localization systems.

Table 1. Free space figures of merit of the measured prototype.

Frequency [MHz]	3744	4243.2	4742.4
Simulated maximum gain [dBi]	6.6	7.0	6.5
Measured maximum gain [dBi]	6.4	7.6	8.0
Simulated FTBR [dB]	9.8	11.4	13.2
Measured FTBR [dB]	11.2	11.0	12.2
Simulated radiation efficiency [%]	96	97	88
Measured radiation efficiency [%]	78	91	87

Acknowledgments

This work was supported by the Fonds de la Recherche Scientifique - FNRS under Grant n° G0F4918N (EOS ID 30452698) and FWO-EOS MUSE-WINET. The experimental measurements reported in this paper are included in the 4TU database under the doi:10.4121/uuid:519aaffd-211e-47d9-ab66-ca62a1c2380b.

References

Adamiuk, G., Zwick, T., & Wiesbeck, W. (2012, July). Uwb antennas for communication systems. *Proceedings of the IEEE*, *100*(7), 2308-2321. doi: 10.1109/JPROC.2012.2188369

Agneessens, S., Castel, T., Van Torre, P., Tanghe, E., Vermeeren, G., Joseph, W., & Rogier, H. (2013). A wearable repeater relay system for interactive real-time wireless capsule endoscopy. In *2013 Proceedings of the International Symposium on Antennas and Propagation* (Vol. 1, pp. 597–600). IEEE.

Agneessens, S., Lemey, S., Vervust, T., & Rogier, H. (2015). Wearable, small, and robust: the circular quarter-mode textile antenna. *IEEE Antennas and Wireless Propagation Letters*, *14*, 1482–1485. Retrieved from `http://dx.doi.org/10.1109/LAWP.2015.2389630`

Alarifi, A., Al-Salman, A., Alsaleh, M., Alnafessah, A., Al-Hadhrami, S., Al-Ammar, M. A., & Al-Khalifa, H. S. (2016). Ultra wideband indoor positioning technologies: Analysis and recent advances. *Sensors*, *16*(5), 36. Retrieved from `https://doi.org/10.3390/s16050707`

Bait-Suwailam, M. M., Labiano, I. I., & Alomainy, A. (2019, March). Effect of textile properties on a low-profile wearable loop antenna for healthcare applications. In *2019 13th european conference on antennas and propagation (eucap)* (p. 1-4).

Bharadwaj, R., Swaisaenyakorn, S., Parini, C. G., Batchelor, J. C., & Alomainy, A. (2017, Dec). Impulse radio ultra-wideband communications for localization and tracking of human body and limbs movement for healthcare applications. *IEEE Transactions on Antennas and Propagation*, *65*(12), 7298-7309. doi: 10.1109/TAP.2017.2759841

Bozzi, M., Georgiadis, A., & Wu, K. (2011). Review of substrate-integrated waveguide circuits and antennas. *IET Microwaves, Antennas & Propagation*, *5*(8), 909-920.

Castel, T., Lemey, S., Agneessens, S., Van Torre, P., Rogier, H., & Oestges, C. (2015). Reliable communication between rescuers during interventions using textile antenna systems. In *2015 IEEE 20th International workshop on Computer Aided Modelling And Design of communication links and networks (CAMAD)* (pp. 135–139). IEEE.

Chatterjee, S., Chatterjee, S., Choudhury, S., Basak, S., Dey, S., Sain, S., ... Sircar, S. (2017, Oct). Internet of things and body area network-an inte-

grated future. In *2017 IEEE 8th Annual Ubiquitous Computing, Electronics and Mobile Communication Conference (UEMCON)* (p. 396-400). doi: 10.1109/UEMCON.2017.8249094

Dierck, A., Rogier, H., & Declercq, F. (2013). A wearable active antenna for global positioning system and satellite phone. *IEEE Transactions on Antennas and Propagation*, *61*(2), 532–538. Retrieved from `http://dx.doi.org/10.1109/TAP.2012.2223441`

Hertleer, C., Van Laere, A., Rogier, H., & Van Langenhove, L. (2010). Influence of relative humidity on textile antenna performance. *Textile Research Journal*, *80*(2), 177–183. Retrieved from `http://dx.doi.org/10.1177/0040517509105696`

Hong, J.-S., & Lancaster, M. J. (1996, Nov). Couplings of microstrip square open-loop resonators for cross-coupled planar microwave filters. *IEEE Transactions on Microwave Theory and Techniques*, *44*(11), 2099-2109.

Hong, Y., Tak, J., & Choi, J. (2016). An all-textile SIW cavity-backed circular ring-slot antenna for WBAN applications. *IEEE Antennas and Wireless Propagation Letters*, *15*, 1995-1999. doi: 10.1109/LAWP.2016.2549578

Kaija, T., Lilja, J., & Salonen, P. (2010, Oct). Exposing textile antennas for harsh environment. In *2010 - MILCOM 2010 Military Communications Conference* (p. 737-742). doi: 10.1109/MILCOM.2010.5680300

Kennedy, T. F., Fink, P. W., Chu, A. W., Champagne, N. J., Lin, G. Y., & Khayat, M. A. (2009, April). Body-worn e-textile antennas: The good, the low-mass, and the conformal. *IEEE Transactions on Antennas and Propagation*, *57*(4), 910-918. doi: 10.1109/TAP.2009.2014602

Khan, Z., Chen, X., He, H., Xu, J., Wang, T., Cheng, L., ... Virkki, J. (2019, Sep.). Glove-integrated passive uhf rfid tagsfabrication, testing and applications. *IEEE Journal of Radio Frequency Identification*, *3*(3), 127-132. doi: 10.1109/JRFID.2019.2922767

Klemm, M., & Troester, G. (2006, Nov). Textile uwb antennas for wireless body area networks. *IEEE Transactions on Antennas and Propagation*, *54*(11), 3192-3197. doi: 10.1109/TAP.2006.883978

Kshetrimayum, R. S. (2009, Mar). An introduction to UWB communication systems. *IEEE Potentials*, *28*(2), 9-13. doi: 10.1109/MPOT.2009.931847

Lazzari, F., Buffi, A., Nepa, P., & Lazzari, S. (2017, May). Numerical investigation of an uwb localization technique for unmanned aerial vehicles in outdoor scenarios. *IEEE Sensors Journal*, *17*(9), 2896-2903. doi: 10.1109/JSEN.2017.2684817

Lee, H., & Choi, J. (2017, Jul). A compact all-textile on-body SIW antenna for IoT applications. In *2017 IEEE International Symposium on Antennas and Propagation USNC/URSI National Radio Science Meeting* (p. 825-826). doi: 10.1109/APUSNCURSINRSM.2017.8072455

Lee, H., Tak, J., Hong, Y., & Choi, J. (2016, Oct). Design of an all-textile antenna integrated in military beret for GPS/RFID applications. In *2016 International Symposium on Antennas and Propagation (ISAP)* (p. 982-983).

Lemey, S., Agneessens, S., & Rogier, H. (2018). Wearable smart objects. *IEEE MICROWAVE MAGAZINE*, *19*(6), 83–100. Retrieved from `http://dx.doi.org/10.1109/MMM.2018.2844030`

Lemey, S., & Rogier, H. (2014). SIW textile antennas as a novel technology for UWB RFID tags. In *2014 IEEE RFID Technology and Applications Conference (RFID-TA)* (pp. 256–260). IEEE.

Lilja, J., Salonen, P., Kaija, T., & de Maagt, P. (2012, Sep). Design and manufacturing of robust textile antennas for harsh environments. *IEEE Transactions on Antennas and Propagation*, *60*(9), 4130-4140. doi: 10.1109/TAP.2012.2207035

Liu, F., Xu, Z., Ranasinghe, D. C., & Fumeaux, C. (2016). Textile folded half-mode

substrate-integrated cavity antenna. *IEEE Antennas and Wireless Propagation Letters*, *15*, 1693-1697. doi: 10.1109/LAWP.2016.2524458

Loss, C., Gonçalves, R., Lopes, C., Pinho, P., & Salvado, R. (2016). Smart coat with a fully-embedded textile antenna for IoT applications. *Sensors*, *16*, 1–13. Retrieved from `https://doi.org/10.3390/s16060938`

Luo, Y., & Look Law, C. (2015, Sep). Robust ultra-wideband direction finding in dense cluttered environments. *IEEE Transactions on Wireless Communications*, *14*(9), 4772-4782. doi: 10.1109/TWC.2015.2425880

Lv, H., Li, W., Li, Z., Zhang, Y., Jiao, T., Xue, H., ... Wang, J. (2014, Nov). Characterization and identification of IR-UWB respiratory-motion response of trapped victims. *IEEE Transactions on Geoscience and Remote Sensing*, *52*(11), 7195-7204. doi: 10.1109/TGRS.2014.2309141

Mandal, B., Mukherjee, B., Chatterjee, A., & Parui, S. K. (2013, Dec). Design of printed body wearable textile antenna for broadband application. In *2013 IEEE Applied Electromagnetics Conference (AEMC)* (p. 1-2). doi: 10.1109/AEMC.2013.7045018

IEEE Standard for Local and metropolitan area networks–Part 15.4: Low-Rate Wireless Personal Area Networks (LR-WPANs). (2011, Sep). *IEEE Std 802.15.4-2011 (Revision of IEEE Std 802.15.4-2006)*, 1-314. doi: 10.1109/IEEESTD.2011.6012487

Minne, K., Macoir, N., Rossey, J., Van den Brande, Q., Lemey, S., Hoebeke, J., & De Poorter, E. (2019). Experimental evaluation of UWB indoor positioning for indoor track cycling. *SENSORS*, *19*, 17. Retrieved from `http://dx.doi.org/10.17632/fkhfjfspkr.1`

Osman, M., Rahim, M., Samsuri, N. A., Elbasheer, M., & Ali, M. (2012, 05). Textile uwb antenna bending and wet performances. *International Journal of Antennas and Propagation*, *2012*. doi: 10.1155/2012/251682

Quintero, G., Zürcher, J.-F., & Skrivervik, A. K. (2011). System fidelity factor: a new method for comparing UWB antennas. *IEEE Transactions on Antennas and Propagation*, *59*(7), 2502-2512. doi: 10.1109/TAP.2011.2152322

Rabah, M. H., Seetharamdoo, D., Addaci, R., & Berbineau, M. (2015). Novel miniature extremely-wide-band antenna with stable radiation pattern for spectrum sensing applications. *IEEE Antennas and Wireless Propagation Letters*, *14*, 1634-1637. doi: 10.1109/LAWP.2015.2415491

Ridolfi, M., Vandermeeren, S., Defraye, J., Steendam, H., Gerlo, J., De Clercq, D., ... De Poorter, E. (2018). Experimental evaluation of uwb indoor positioning for sport postures. *SENSORS*, *18*(1). Retrieved from `http://dx.doi.org/10.3390/s18010168`

Rogier, H., Agneessens, S., Castel, T., Lemey, S., Declercq, F., Vanveerdeghem, P., ... Joseph, W. (2014). Novel wearable antenna systems for high datarate mobile communication in healthcare. In *2014 EAI 4th International Conference on Wireless Mobile Communication and Healthcare (MOBIHEALTH)* (pp. 188–191). Retrieved from `http://dx.doi.org/10.4108/icst.mobihealth.2014.257274`

Samal, P. B., Soh, P. J., & Vandenbosch, G. A. E. (2014, Jan). UWB all-textile antenna with full ground plane for off-body WBAN communications. *IEEE Transactions on Antennas and Propagation*, *62*(1), 102-108. doi: 10.1109/TAP.2013.2287526

Sanz-Izquierdo, B., Batchelor, J., & Sobhy, M. (2007, 05). Compact uwb wearable antenna. In (p. 121 - 124). doi: 10.1109/LAPC.2007.367446

Shen, H., Xu, C., Yang, Y., Sun, L., Cai, Z., Bai, L., ... Huang, X. (2018, Oct). Respiration and heartbeat rates measurement based on autocorrelation using IR-UWB radar. *IEEE Transactions on Circuits and Systems II: Express Briefs*, *65*(10), 1470-1474. doi: 10.1109/TCSII.2018.2860015

Skrivervik, A. K., & Marrocco, G. (2015). Guest editorial: Special cluster on antennas for wireless body area networks. *IEEE Antennas and Wireless Propagation Letters*, *14*, 1471-1473. doi: 10.1109/LAWP.2015.2457531

Van Baelen, D., Lemey, S., Verhaevert, J., & Rogier, H. (2018). A novel manufacturing process for compact, low-weight and flexible ultra-wideband cavity backed textile antennas. *MATERIALS*, *11*(1), 17. Retrieved from `http://dx.doi.org/10.3390/ma11010067`

Van Baelen, D., Lemey, S., Verhaevert, J., & Rogier, H. (2019, Mar). Improved fabrication methodology for foldable all-textile cavity-backed slot antennas. In *2019 URSI Asia Pacific Radio Science Conference (AP-RASC)* (p. 1-4). doi: 10.23919/URSIAP-RASC.2019.8738601

Van den Brande, Q., Lemey, S., Vanfleteren, J., & Rogier, H. (2018). Highly-efficient impulse-radio ultra-wideband cavity-backed slot antenna in stacked air-filled substrate-integrated-waveguide technology. *IEEE Transactions on Antennas and Propagation*, *66*(5), 2199-2209.

Yan, S., Poffelie, L. A. Y., Soh, P. J., Xuezhi Zheng, & Vandenbosch, G. A. E. (2016, Apr). On-body performance of wearable UWB textile antenna with full ground plane. In *2016 10th European Conference on Antennas and Propagation (EuCAP)* (p. 1-4). doi: 10.1109/EuCAP.2016.7481477

Yimdjo Poffelie, L. A., Soh, P. J., Yan, S., & A. E. Vandenbosch, G. (2016, Feb). A high-fidelity all-textile UWB antenna with low back radiation for off-body WBAN applications. *IEEE Transactions on Antennas and Propagation*, *64*(2), 757-760. doi: 10.1109/TAP.2015.2510035

Zhong, J., Kiourti, A., Sebastian, T., Bayram, Y., & Volakis, J. L. (2017). Conformal load-bearing spiral antenna on conductive textile threads. *IEEE Antennas and Wireless Propagation Letters*, *16*, 230-233. doi: 10.1109/LAWP.2016.2570807

Zhu, S., & Langley, R. (2009, April). Dual-band wearable textile antenna on an ebg substrate. *IEEE Transactions on Antennas and Propagation*, *57*(4), 926-935. doi: 10.1109/TAP.2009.2014527

Zwirello, L., Reichardt, L., Li, X., & Zwick, T. (2012, Mar). Impact of the antenna impulse response on accuracy of impulse-based localization systems. In *2012 6th European Conference on Antennas and Propagation (EUCAP)* (p. 3520-3523). doi: 10.1109/EuCAP.2012.6206489